Proceedings World Geothermal Congress 2020+1
Reykjavik, Iceland, April - October 2021

Modeling Neutralization of Acid Fluids in the Biliran Geothermal Field, Philippines

John Paul A. Mendoza, Maria Ines Rosana Balangue-Tarriela and Mark H. Reed

University of the Philippines Baguio, Governor Pack Road, Military Cut Off, Baguio City, Philippines 2600

jamendoza5@up.edu.ph

Keywords: CHIM-XPT, geochemical modeling, Biliran, water-rock interaction

ABSTRACT

Using numerical geochemical modelling through FORTRAN programs GEOCAL, SOLVEQ-XPT and CHIM-XPT (2016), the hydrogeochemical model (neutralization of magmatic-acidic fluids by extensive water-rock interaction) of Biliran geothermal field was tested. Water-rock interaction (WRI) was simulated by incrementally titrating an andesitic wall rock into the 1 kg of the magmatic-acidic water at the reservoir temperature (350°C). Results of the modeling showed significant change in pH (1.5 to 5.6) at the end of the rock titration with the neutralization process resulting from the precipitation and/or dissolution of alteration minerals including rutile, quartz, calcite, epidote, feldspars, chlorite end-members, apatite and pyrite. Alteration assemblages of rocks intersected by the Biliran drill holes using petrographic analysis and XRD conform well to the predicted alteration minerals while differences in the observed and predicted mineralogy may be attributed to the oversimplification of the modeled scenarios..

1. INTRODUCTION

Energy generation from geothermal systems can be considered as a result of heat mining by water (or steam) in hot rocks. Water-rock interaction in geothermal systems not only mines heat but also results to irreversible changes in the composition of both the fluid and the rock (Harvey, 2013). As shown in Figure 1, hydrothermal alteration is produced when an initial hot fluid F1 passes through a rock of R1 mineralogy altering it and producing R2 simultaneously changing the fluid composition into F2. The alteration may be pervasive both vertically and laterally with patterns distinct to the prevailing physical and chemical conditions (Reed, 1994). Unstable primary mineral phases are converted gradually into a secondary alteration assemblage (Giggenbach, 1981).These alteration assemblage provide information regarding the temperature, pressure, fluid type (acidity, ionic ratios, etc.), porosity, permeability, redox potential and other parameters that characterize the geothermal system (Reyes, 1990). Consequently, change in the fluid composition is achieved by the utilization of ions in the water for the formation of the alteration assemblage which would enable us to trace the evolution of the fluids and the geothermal system (Zhang, 2001). The fluid chemistry and chemical geothermometers provide information about processes in the system including estimated resource temperature at depth, origin of resource, mixing of aquifers, pathway of discharge, sources of recharge, fluid potential for corrosion or scaling and the resource temperature which are essential to the exploitation of geothermal resources (Harvey, 2013).

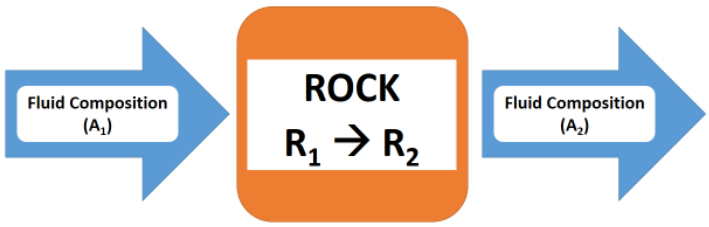

Figure 1: Conceptual Model of Hydrothermal Alteration. A hot fluid with composition A1 passing through a rock (R1) would change the both the fluid and rock's composition into A2 and R2 simultaneously.

On the basis of fluid and gas chemistry obtained from the Biliran exploratory wells, along with previous studies centered in their alteration mineralogy (Pagado et al., 1993; Licup and Omac, 2014; Reyes, 2015), the current hydrogeologic model of the Biliran geothermal field suggests that the neutral chlorite fluids obtained in BN-1, BN-2, and BN-6 are products of the neutralization of acidic fluids due to intensive water-rock interaction. Thus, it is important to look closely into this particular process. This study in particular, aims to model the water-rock interaction of the Biliran geothermal system using fluid chemistry data and well cuttings. It specifically aims to (1) predict the alteration mineral assemblage that may form at various water-rock ratio, (2) identify the extent and intensity of alteration in the hydrothermal system and (3) compare these modeled simulations with real-life observations based on well cuttings. Results of the study may aid in identifying possible problems during the exploitation of the resource in terms of changes in fluid chemistry, which may cause corrosion of well casings, or precipitation of scale minerals possibly causing blockages in the wells. However as in typical modeling simulation, some assumptions which will be used may not always hold true for certain conditions and will depend on the characteristics of the hydrothermal system. Other relevant data including well and gas chemistry have been sampled and analyzed by the host company, Biliran Geothermal Inc., along with some geologic data (geomorphology based on LIDAR, structural data, drilling and logging of well cuttings etc.)..

2. STUDY AREA

Biliran Island is located at approximately 1,115 km southwest of Metro Manila and 45 km northwest of the Tongonan geothermal power plant in Leyte, eastern Visayas region. It is characterized by a northwest-southeast elongated volcanic terrain with the presence

of well-defined craters/collapse features, fumaroles, boiling mud pools, hot spring and extensive altered grounds. Most of the volcanic vents marked by craters on top of domes, flanks or caldera (Figure 2) are situated at high elevations exceeding a kilometer in height.

2.1 Geology of Biliran Island

Quaternary volcanoes related to the subduction of the Philippine Sea Plate along the Philippine Trench constitute the majority of Biliran Island. The island is also situated a few kilometers east of the left-lateral Philippine Fault which plays a major role in the structural framework of the island. These factors created favorable conditions for a possible geothermal system (Pagado et al., 1995).

Known rock formations identified in the island include (1) a metamorphic basement, (2) the Balacson Volcanics (BnV) and (3) Caibiran Sedimentary Formation (CSF). The pre-Miocene schistose basement have no surface exposures and were only encountered in the last 15-m of drillhole well BN-1. A sample from the bottom hole was identified by Reyes (1982) as muscovite-chlorite-albite-quartz augen schist. The basement is possibly Cretaceous based on similarities with the exposed metamorphic rocks in Cebu and Samar. The Balacson Volcanics is only exposed in the Northwestern tip of the island (municipality of Kawayan) and was not intercepted by any wells drilled. It consists of N-S folded scoriaceous pyroxene basalt grading to basalt agglomerates. It is possibly coeval with the Lower to Middle Central Highland Volcanics of Leyte and predates CSF. Encountered in BN-1, the 344 meter thick Late Miocene to Early Pliocene (Reyes and Ordonez, 1970) CSF consists of fossiliferous calcisiltie to calcarenites and calcareous sandstone-siltstone (FEDCO, 2009).

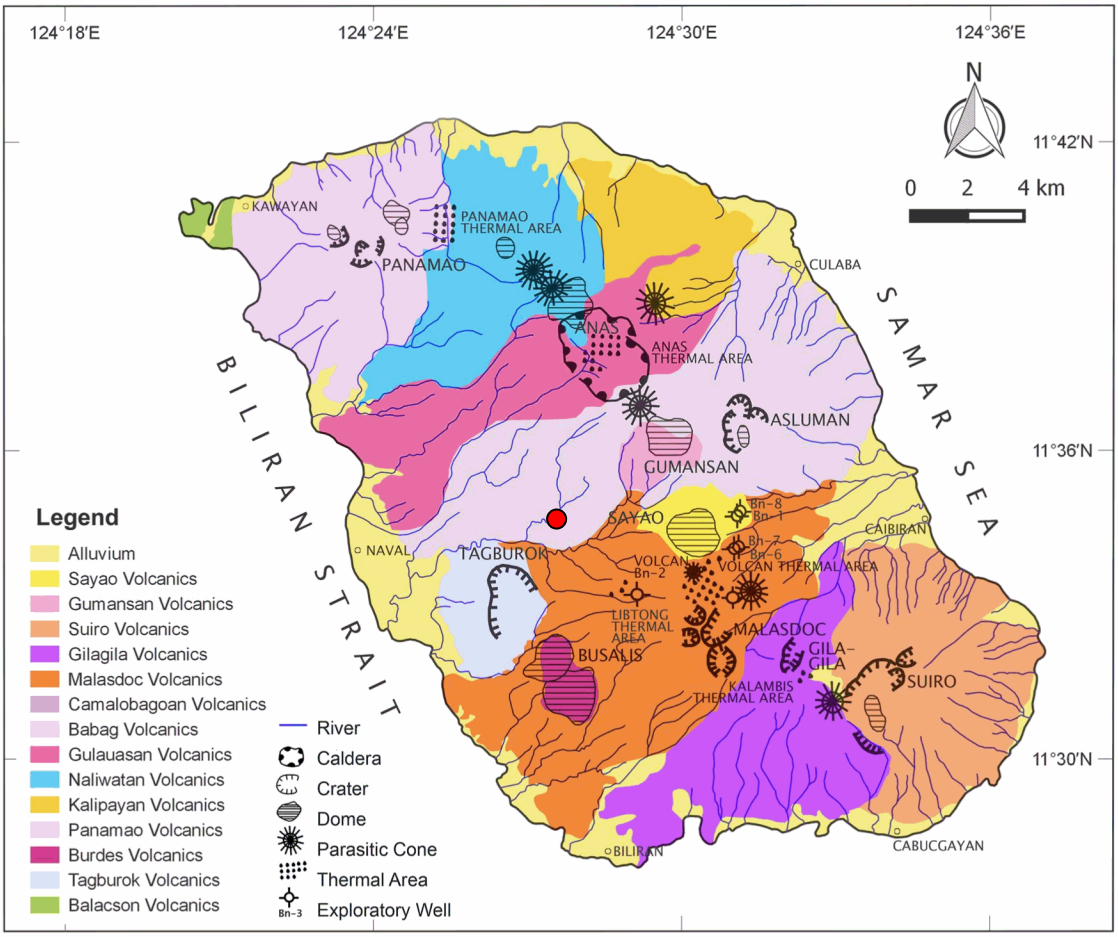

Figure 2: Simplified Geologic Map of Biliran Island (Modified from FEDCO, 2009).Distribution of volcanic features which follow a hazy "Z" like pattern is also shown in the map. Red dot on the map indicates location of rock samples taken in the field.

Overlying these units are the volcanic deposits of the Biliran Volcanic Complex (BVC) dominating the majority of the island. Early explorations done by PNOC-EDC as stated by Pagado et al. (1995) identified 9 volcanic centers which extended to at least 13 groups (Figure 2) after the re-evaluation done by Biliran Geothermal Incorporated (BGI) using LIDAR accompanied by ground-truthing in the identified structures. The volcanic centers are of either single or several deposits and have at least 56 volcanic units. Volcanic edifices occur as simple to compound stratocones and domes which have a uniform and narrow range of composition. Most of the rock units were classified as andesite lava flows, pyroclastics and lahar deposits grading from a more basic to less basic composition suggesting magmatic differentiation during its coalescing short-lived volcanic activities. The volcanic units include Panamao, Tagburok, Busales, Kalipayan, Naliwatan, Gulauasan, Babag, Camalobagoan, Malasdoc, Gilagila, Suiro, Gumansan and Sayao. Their relative ages (Figure 3) were inferred based on morphological, mineralogic and stratigraphic relationships since no radiometric dating is available (FEDCO, 2009). The Maasdoc Volcanics (MaV) hosts the Vulcan-Libtong thermal areas where three PNOC-EDC exploratory wells were drilled. MaV consists of pyroxene basalts, pyroxene andesites to hornblende-bearing pyroxene andesites.

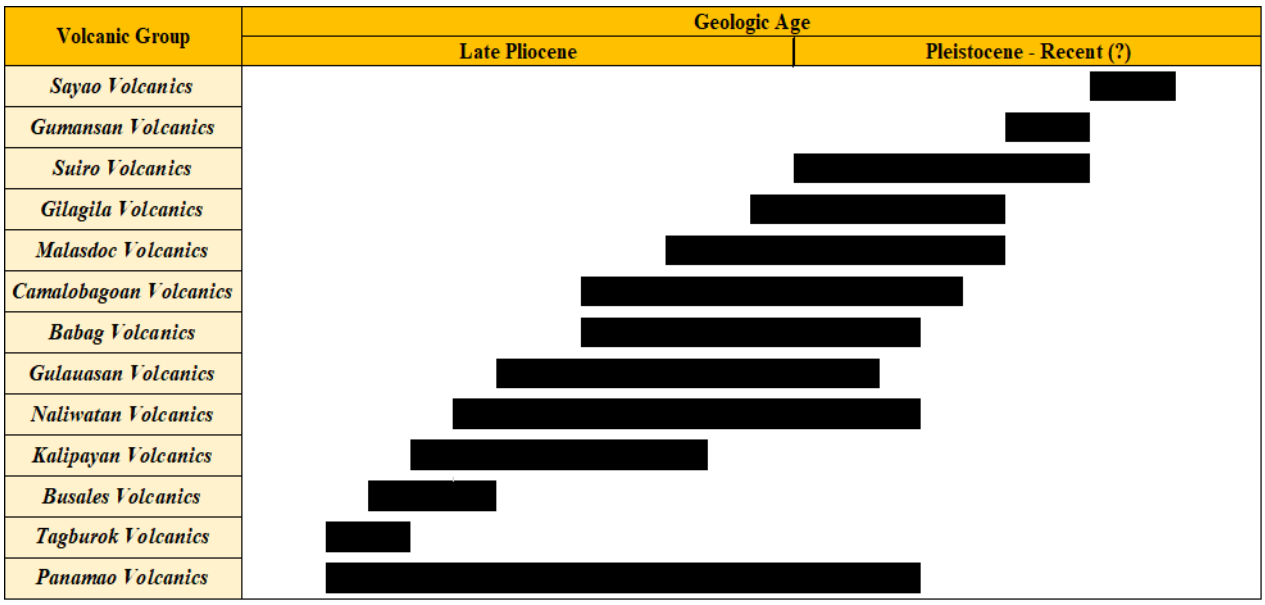

Figure 3: Relative ages and length of volcanic activities of the different units in the Biliran Volcanic Complex. The relative ages were determined from field evidences (Modified from FEDCO, 2009).

2.2 Timeline of Exploration

Exploration in the Biliran Island began in 1979 with the inventory of surface hydrothermal features under the PNOC-EDC and KRTA of New Zealand. Several geothermal systems can be found in the island based on geology, geochemistry and geophysical data. Most of the thermal manifestations in the island are associated with the young volcanic centers and associated structures (FEDCO, 2009). Secondary mineral assemblages were found in three thermally altered ground with warm springs (Panamao, Anas and Kalambis) which are indicative of conditions hotter than present, thus having dying systems (Apuada and Sigurjonsson, 2008).

Investigative work including geology, geochemistry and geophysical surveys lead to drilling three exploratory wells (BN-1, -2 and -3) from 1982-1983 in the Vulcan area, the site of the most impressive identified thermal area in the island. Vulcan area which is in close proximity to Mt. Sayao hosts umerous solfataras, hotsprings and bubbling pools with intensely altered grounds containing an acidic mineral assemblage. Hotsprings progressively decrease in temperature and pH away from the Vulcan area (Pagado et al., 1995) Neutral Cl fluids with TSi02 temperatures of 250ºC and 210ºC were encountered on BN-1 and -2 respectively. Corrosive acid Cl-SO_4 waters (pH=3.0) with very high SO_4, Mg and Fe were obtained from BN-3 located near the Vulcan point (Apuada and Sigurjonsson, 2008).

Neutral chloride fluid penetrates the reservoir but acid component from magmatic sources introduced into the postulated upflow region poses a major obstacle to development along with site logistics. High temperatures at exploitable depths appear to be confined to a small area so no further activity were taken until 1992 (Apuada and Sigurjonsson, 2008).

A series of geological survey was undertaken by the PNOC-EDC Geothermal Division to reassess the significance of the geothermal areas and find alternative models to be used for assessing the feasibility of development (Pagado et al., 1995). However, despite the additional surface geoscientific studies, no significant changes were made to the existing modeI so no activities were undertaken since then. In 2008, the DOE awarded the geothermal service contract to Biliran Geothermal Incorporated (BGI). Reassessment conducted by FEDCO revealed a 32 km^2 geothermal resource area centered in Malasdoc and Gilagila volcanoes where Vulcan-Libtong-Kalambis thermal areas are located. Other resource areas related to Panamao and Naliwatan-Gulausan volcanoes in the north were also identified (FEDCO, 2009). Additional surface exploration were undertaken by BGI from 2012 to 2014 including LIDAR digital terrain model (DTM), ground truthing of inferred faults, resampling of fumaroles and mapping the nature of altered grounds between Vulcan Dako and Libtong thermal areas (Bjornsson and Sarmiento, 2015). From 2013 to 2014, a total of 5 directionally drilled wells (BN-4, BN-5, BN-6, BN-7 and BN-8) averaging to 2 km deep were drilled (as shown in Figure 2) to further assess the generating capacity of the prospect. A power capacity potential of more than 200 MW (production load of 10 MW/km^2) for the project is expected based on the results of the new drilling, an increase over previously expected potential based on a resistivity anomaly.

2.3 Biliran Geothermal System

At least four major hydrothermal systems are identified on the more evolved volcanoes along the EVB based on geochemical, geological and geophysical data. Three of these are regarded as waning geothermal systems namely Panamao, Anas and Kalambis. The active Vulcan-Libtong thermal area, located near Mt. Sayao and Vulcan domes (Figure 2) hosts a volcano-magmatic geothermal system (Apuada and Sigurjonsson, 2008). Thermal manifestations include solfataras, hot springs, bubbling pools and completely altered country rocks containing an acidic assemblage. These features are all located along the highly dissected Caibiran divide (Pagado et al., 1995).

Away from the Vulcan area, temperature of hot springs progressively decline along with the increase in pH. Drilling results showed a similar trend with highest temperature reaching 332°C measured at BN-3 while drastically dropping (210-240°C) at BN-1 (3 km to the North) and BN-2 (3.75 km to the west). These wells mark the outer limits of the suitable temperature at exploitable depths of the

prospect. The neutral Cl-brine from these wells evolved from acidic fluids through neutralization by intensive water-rock interaction as the fluid migrates laterally. Fluid discharge compositions and isotopes retained the signatures of the original magmatic vapors particularly for BN-3 where acid fluids are suggested to upflow (Figure 4). From the Vulcan area, hot fluids flow outwards and emerge on the surface along faults and lithologic boundaries as observed in Panlahuban and Bunot thermal springs to the west and Mohon and Villavicenta springs to the east (Apuada and Sigurjonsson, 2008).

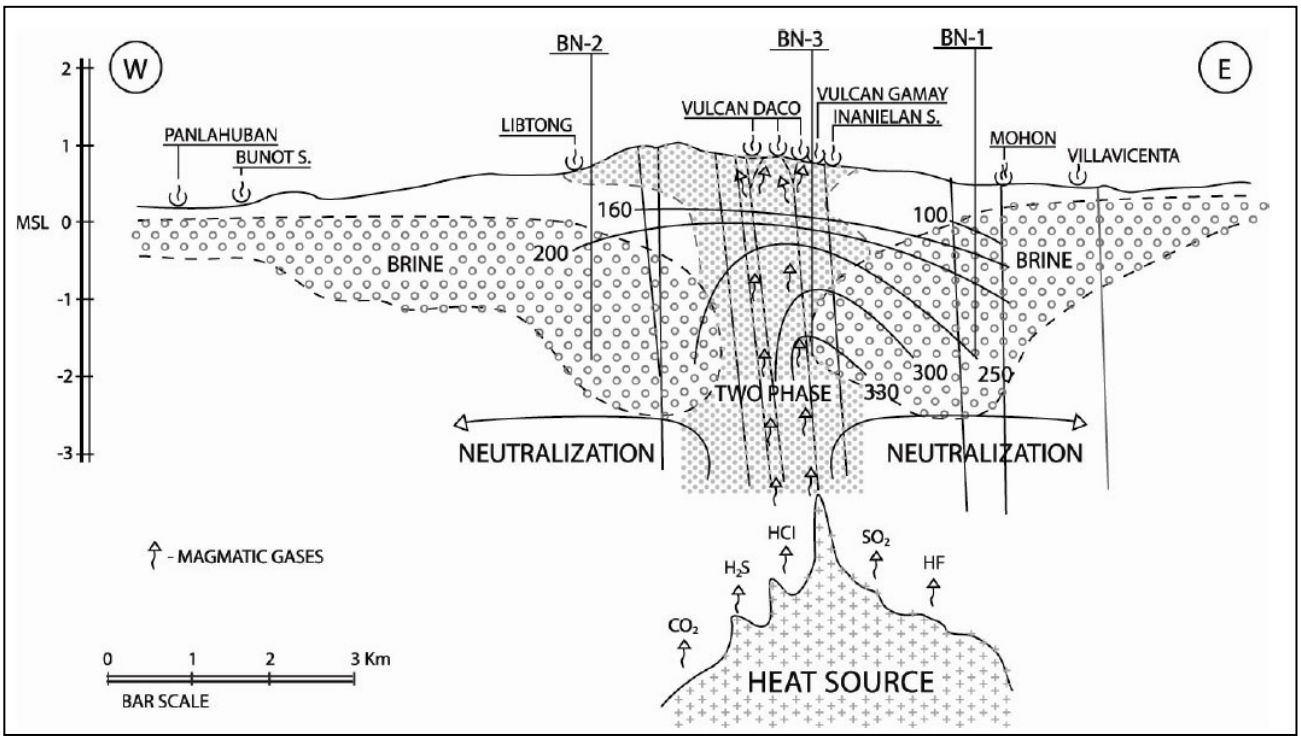

Figure 4: Geothermal Model of Vulcan-Libtong Area (taken from Apuada and Sigurjonsson, 2008). A small partially molten magmatic body heats up the system along with the release of magmatic gases and hot acidic fluids as observed in the Vulcan thermal areas. However, progressive water-rock interaction neutralizes the water as it migrates into the eastern and western side as seen in Villavicenta and Bunot areas.

The Vulcan fault (Figure 4) serves as the main conduit of magmatic gases from the heat source to the surface as manifested by numerous thermal features along its trace (Apuada and Sigurjonsson, 2008). A small partially molten magmatic body at around 10 km or more is postulated to supply the heat to the system (Pagado et al., 1995). According to Ruaya's (1981) model as stated by Pagado et al. (1995), the ascending magmatic gases condense forming acid-sulfate fluids which eventually mix with groundwater and progressively neutralized as they flow outwards through highly porous passageway and interact with the country rocks.

3. MODELING USING CHIM-XPT: CONCEPTS, APPROACH AND ASSUMPTIONS

Numerical calculations will be executed using the FORTRAN program CHIM-XPT (successor of CHILLER-XPT) by Reed (1992) along with accompanying tool called MINTAB. These programs run in any basic command-line interpreters such as command prompt in Windows and uses minimal computer random-access memory (RAM). Program CHIM-XPT computes equilibrium distribution of components among aqueous species, minerals and gases at changing composition (X), pressure (P) and temperature (T). It uses equilibrium constants in its SOLTHERM-XPT thermodynamic database. Unlike other geochemical modeling softwares, modeling conditions of up to 600°C and 5 Kbar can be examined (Reed et al., 2012). Complex processes including cooling hydrothermal solutions, reaction of solutions with rock, fluid-fluid mixing (meteoric, seawater, geothermal or any type of fluids), gas titrations, boiling, adiabatic decompression, condensation, evaporation as well as sedimentary (e.g. diagenesis) and metamorphic processes may be modelled using this program (Reed et al., 2012).

Modeling simultaneous equilibria in aqueous-mineral- gas system applies a technique known as the Newton-Rhapson method (equation 1) which simultaneously solves a set of 30 to 50 non-linear equations described by mass action, mass balance and enthalpy balance (Reed, 1992).

$$x_{n+1} = x_n - \frac{f'(x_n)}{f(x_n)} \tag{1}$$

This technique of root approximation makes use of the derivative of the function. In the event that the derivative cannot be determined analytically, it is approximated by the difference quotient. With the use of initial trial values for unknown variables (manually inputted and are usually five to six orders of their correct values), this method takes the partial derivatives of the mass action, mass balance and/or enthalpy balance equations then setting up these derivatives in a matrix that is repeatedly solved incrementally. In doing so, an improved value of the unknown variable is estimated for each iteration. A more detailed discussion on these equations and the calculation method is presented by Reed (1998).

The mass action equations for aqueous species which involves complexes, ion pairs and redox species uses an extended Debeye-Huckel equation which takes into account non-ideality of aqueous salt solutions (Hegelson et al., 1981 as stated by Reed, 1992). For aqueous-solid equilibria (pure minerals and mineral solid solutions), additional mass action equations are solved for each currently saturated mineral or solid solution end member. Aqueous-gas equilibria is also solved taking into account the non-ideality and non-ideal mixing of H_2O, CO_2, CH_4, H_2 and H_2S (Spycher & Reed, 1988) while treating S_2, SO_2, Hg, HCl and HF as ideal gases (Reed, 1992).

Water-rock interaction was simulated by incrementally titrating the wall rock into the 1 kg of the initial reservoir water at the reservoir temperature. To prevent boiling, pressure was kept at slightly above saturation with the assumption that minerals formed were left in contact with the solution. In this way, precipitation and re-dissolution of minerals is allowed depending on the changes happening in the fluid chemistry as the rock titration intensifies. A similar method was utilized in several studies particularly in Philippine geothermal fields such as in Tongonan (Balangue-Tarriela, 2004; Cabahug and Angcoy, 2013) and Mt. Labo in the Bicol Peninsula (Bartolo and Reed, 2015).

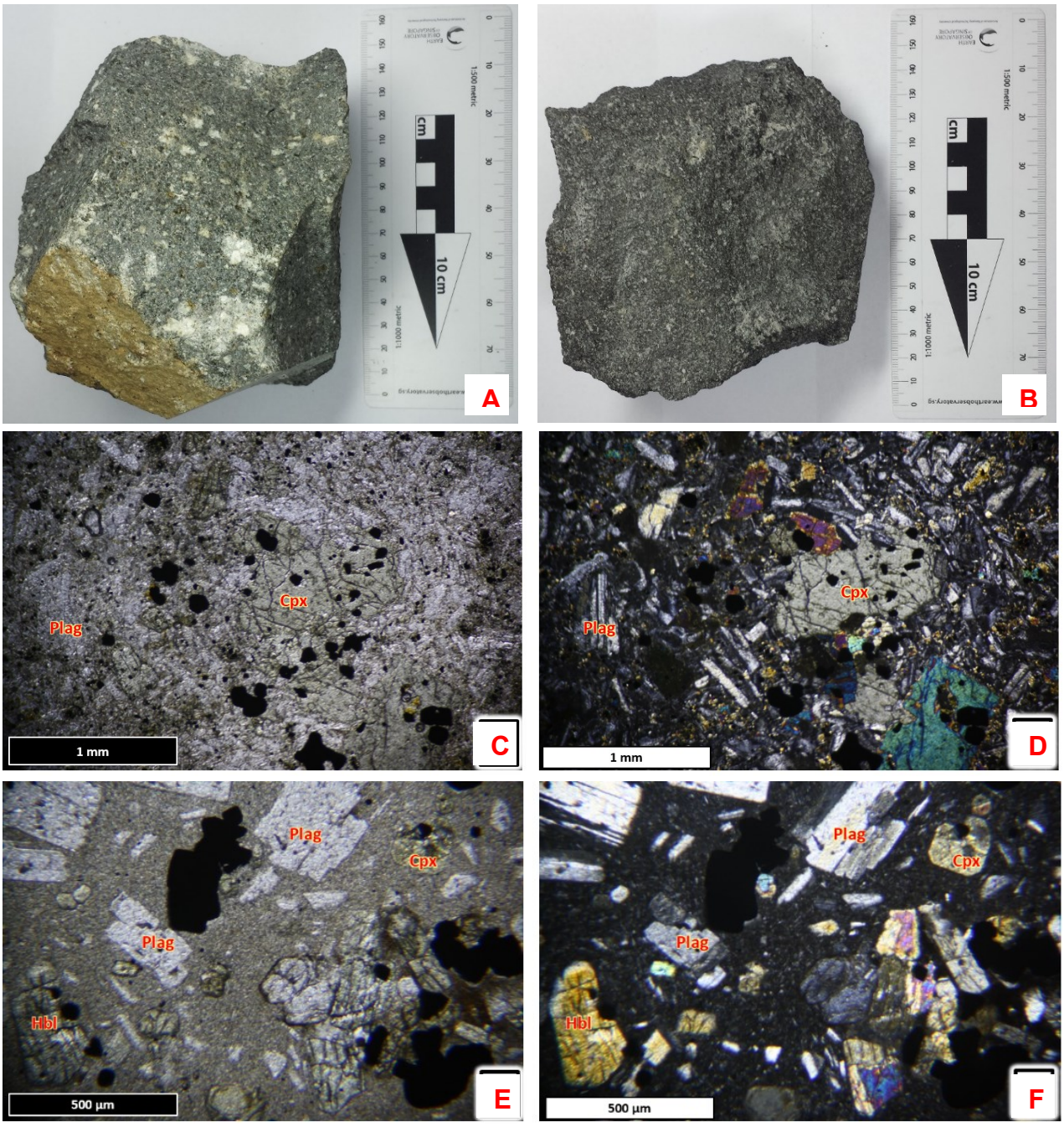

Figure 5: Relatively fresh Biliran andesite samples obtained along the Naval-Caibiran cross-country road. A) Hand sample specimen BN15-01 B) Hand sample specimen BN15-02 C) BN15-01 thin-section in Plane-polarized light (PPL) D) BN15-02 thin-section in cross-polarized light (XPL) E) BN15-02 thin-section in Plane-polarized light (PPL) F) BN15-02 thin-section in cross-polarized light (XPL).

Well cuttings and well cores (if available) despite being the country rocks are hydrothermally altered to some degree so a representative rock in the form of a relatively fresh andesite was used since the geothermal area is hosted near the Sayao and Vulcan

dome which consists of mostly of andesites. Two rock samples (namely BN15-01 and BN15-02) were taken from two separate outcrops roughly 50 meters away from each other along the Naval-Caibiran Cross Country road in brgy. Lucsoon, Naval situated a few kilometers northwest of the geothermal concession site. The sample location for sample BN15-02 is shown in Figure 2 where Babag Volcanics (BbV), a member of the BVC is spread out. According to FEDCO (2009), BbV is characterized by hornblende-bearing pyroxene andesite to pyroxene andesite lava flows, volcanic breccias and lahars.

Sample BN15-01 shows an aphanoporphyritic texture with phenocrsyst dominated by pyroxene (0.5-2 mm) and lesser amounts of plagioclase (0.5-3 mm) surrounded by a gray (intermediate) phenocryst (Figure 5A). Weak alteration of the mafic phenocrysts are also observed. Under the petrographic microscope, the sample appears to be dominated by subhedral to euhedral plagioclase crystals with some of which exhibiting zoning and sieve textures. The mafic minerals on the other hand are identified as dominantly anhedral to subhedral crystals of clinopyroxene (Cpx) and orthopyroxene (Opx) with most being altered to some extent (Figure 5D). Opaque minerals were also observed in significant amount in the sample (3-5%). On the other hand, sample BN15-02 also shows an aphanoporphyritic texture (Figure 5B). The groundmass (70%) appear to have a darker color (dark gray) close to a basaltic color index with plagioclase (0.5-3 mm) as the dominant phenocryst as compared to BN15-01. Under the microscope (Figure 5E and F), a cryptocrystalline texture was observed. Microphenocrysts are mostly euhedral plagioclase crystals along with fewer mafic minerals dominated by mostly euhedral to subhedral Cpx were along with minor hornblende (Hbl) crystals. Minor degree of alteration were also observed for the mafic minerals. Comparing the two samples, BN15-01 appear have lighter color with larger crystals (2x) under the microscope and more abundant opaque minerals. Despite these textural and minor mineralogical differences, the rocks were identified mainly as (porphyritic) andesites (based on the dominance of plagioclase and minor occurrence of the mafic minerals) following the IUGS classification (Le Bas & Streckeisen, 1991). In summary, most of the characteristics of these samples are similar to the description of the rocks from BbV member of BVC.

The rocks were subjected to x-ray fluorescence analysis to determine the quantitative bulk elemental composition of the rock (Table 1). The analysis was done at Kyushu University, Fukuoka Prefecture, Japan. Based on the major element composition, the samples were identified as dacite (BN15-02) and andesite (BN15-01) using the Total alkali-silica plot (Lemaitre, 2002) as shown in Figure 6. In particular, BN-15-01 shows significant similarity and closeness to the value of the average andesite. Unaltered samples from the main host rocks of BGC are not available. Thus, this particular sample was used to react with the fluids in the preceding section. Despite not being the direct host rocks of the Biliran geothermal wells, the BbV has very close resemblance to MaV in terms of lithology and age of formation (Figure 3). Aside from this, MaV samples particularly nearest the upflow region has been hydrothermally altered intensely thus changing its original chemical composition. Also, as stated above, BN15-01 is has close similarities to the average andesite composition thus, making it safe to use for the model.

Table 1: Chemical Composition (major and minor elements) of the Biliran samples. Average basalt and andesite composition were adopted from LeMaitre (1976, as stated by Winter, 2001).

	mass %									
Sample Name	**SiO_2**	**TiO_2**	**Al_2O_3**	**FeO**	**MnO**	**MgO**	**CaO**	**Na_2O**	**K_2O**	**P_2O_2**
BN 15-02	63.96	0.585	15.96	5.412	0.145	1.96	5.96	2.42	2.23	0.217
BN 15-01	57.61	0.825	18.04	7.552	0.168	2.99	8.5	2.27	1.22	0.216
Ave. Andesite	57.94	0.87	17.02	4.04*	0.14	3.33	6.79	3.48	1.62	0.83
Ave. Basalt	49.20	1.84	15.74	7.13*	0.20	6.73	9.47	2.91	1.10	0.95

*Fe_2O_3 was measured with values 3.27 for andesite and 3.89 for basalt

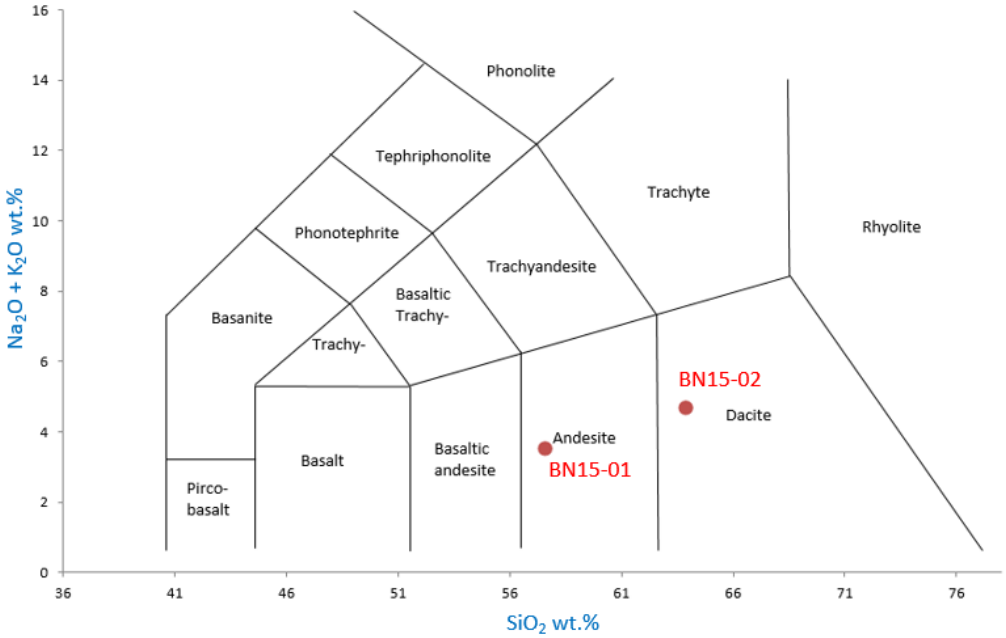

Figure 6: Total Alkali-Silica Diagram (after Le Maitre, 2002) Plots of Biliran Samples

To simulate the interaction between the magmatic acidic water at depth, a theoretical water is used for the modeling. This water which is shown in Table 2 is based on the acidic fluids of Mahanagdong in Leyte Geothermal field and was further acidified by mixing with 75% HCl and 25% H_2SO_4 to obtain an initial pH of 1.5 (Reed, pers comm). This step is necessary since it is impossible to get a representative sample of the magmatic-acidic fluids at depth and no downhole chemistry sample is available from BN-6 and BN-7. A sample run file is shown in Appendix A showing an estimated reservoir temperature of 350°C with a starting 1:0 water-rock ratio incrementally changing at 0.001 (<step increm>) up to a ratio of 0.01 (<step limit>). Several pick-up runs were done until the maximum concentration of 10,000 grams of andesite was reacted. A slight modification was done to the water by adding a small concentration values (in moles) of chemical species Al^{3+}, Fe^{2+}, Mn^{2+}, HPO_4^{2-} and $Ti(OH)_4$ since these species are present in the concentration obtained for the rock sample to be reacted.

Table 2: Composition of the theoretical acidic fluid used for the rock titration model.

Component Species	Total Moles
H^+	1.015178
H_2O	1.379634
Cl^-	0.687273
$SO4^{2-}$	0.126002
HCO_3^-	0.2498
HS^-	7.67E-03
H_4SiO_4	1.31E-02
$*Al^{3+}$	1.00E-21
Ca^{2+}	4.57E-05
Mg^{2+}	7.24E-03
$*Fe^{2+}$	1.00E-13
K^+	1.24E-02
Na^+	0.152
$*Mn^{2+}$	1.00E-21
F^-	8.11E-05
$*HPO4^{2-}$	1.00E-13
$NH4^+$	2.64E-03
H_3BO_3	2.97E-03
$*Ti(OH)_4$	1.00E-13
*trial values were inserted since the andesite to be reacted to this water contains significant concentration of these species.	

4. RESULTS AND DISCUSSION

Figure 7 shows the result of the water-rock (w/r) interaction between the andesite and the acidic fluids. The stacked graphs shows similar abscissa in grams of andesite starting at 0.01 to 10000 grams from left to right thus, a larger water-rock ratio going to the right side of the figure. The ordinates on the other hand shows different variables observed for the model such as alteration minerals in log moles (Figure 7A), total molality of major component species (Figure 7B) and the gas phase composition in log moles (O_2 and NO_2 gas off scale at the bottom in Figure 7C).

A striking increase in number of precipitating minerals can be observed in Figure 7A. At a very small w/r ratio, initial precipitation of small amounts of rutile (TiO_2) is produced. This reaction is expected since rutile only requires Ti and OH ions in order to be produced. This is then followed by the precipitation of alunite (at 0.05 grams rock) and quartz (at 0.5 grams rock). Change in pH is very minute during the precipitation of these three minerals up to around 10 grams of andesite reacted thus serving as buffers since they control the activity of H+ to be consumed as shown in equation 2. The amount of these minerals increases as the w/r ratio also increases.

$$KAl_3(OH)_6(SO_4)_2 + 6H^+ + Ti(OH)_4 = TiO_2 + K^+ + 2SO_4^{2-} + 3Al^{3+} + 8H_2O \quad (2)$$
(alunite, s) (aq) (aq) (rutile, s)(aq) (aq) (aq) (aq)

At around 20 grams, anhydrite and andalusite forms along with a more noticeable change in pH. Alunite production stops at roughly around 60 grams of rock reacted followed by a more drastic change in pH up to 100 grams of rock. Production of anhydrite consumes Ca^{2+}, SO_4^{2-}, H^+ ions thus the decrease in concentration and increase in pH as seen in Figure 7B. The increase in pH is mirrored by the decreasing pattern in Ca^{2+} and SO_4^{2-} (from alunite) which goes into the anhydrite. This may be seen in the reaction between these minerals as shown in equations 3 and 4.

$$KAl_3(OH)_6(SO_4)_2 + H_4SiO_4 \rightarrow Al_2SiO_5 + K^+ + 2SO_4^{2-} + Al^{3+} + 5H_2O \text{ and} \quad (3)$$
(alunite, s) (qtz, s) (and, s) (aq) (aq) (aq) (aq)

$$KAl_3(OH)_6(SO_4)_2 + 6H^+ + Ca^{2+} \rightarrow CaSO_4 + K^+ + 2SO_4^{2-} + 3Al^{3+} + 6H_2O \quad (4)$$
(alunite, s) (aq) (aq) (anh, s) (aq) (aq) (aq) (aq)

The change in pH (now at 3.5) becomes more gradual again starting at around 100 grams (Appendix B). At this w/r ratio, apatite ($Ca_5(PO_4)_3(OH)$), pyrite (FeS_2) and hematite (Fe_2O_3) are simultaneously produced (note that apatite is produced up to the maximum amount of rock reacted). This is then immediately followed by formation of chlorite solid solution end-members (daphnite, clinochlore and minor amounts of chlorite-Mn) along with a slight change in pH. Hematite is then replaced by Chloritoid-Fe (equation 5; Figure 7A; Appendix B). At this w/r ratio, change in pH is mainly controlled by HS^- and SO_4^{2-} showing opposite trends in Figure 7B.

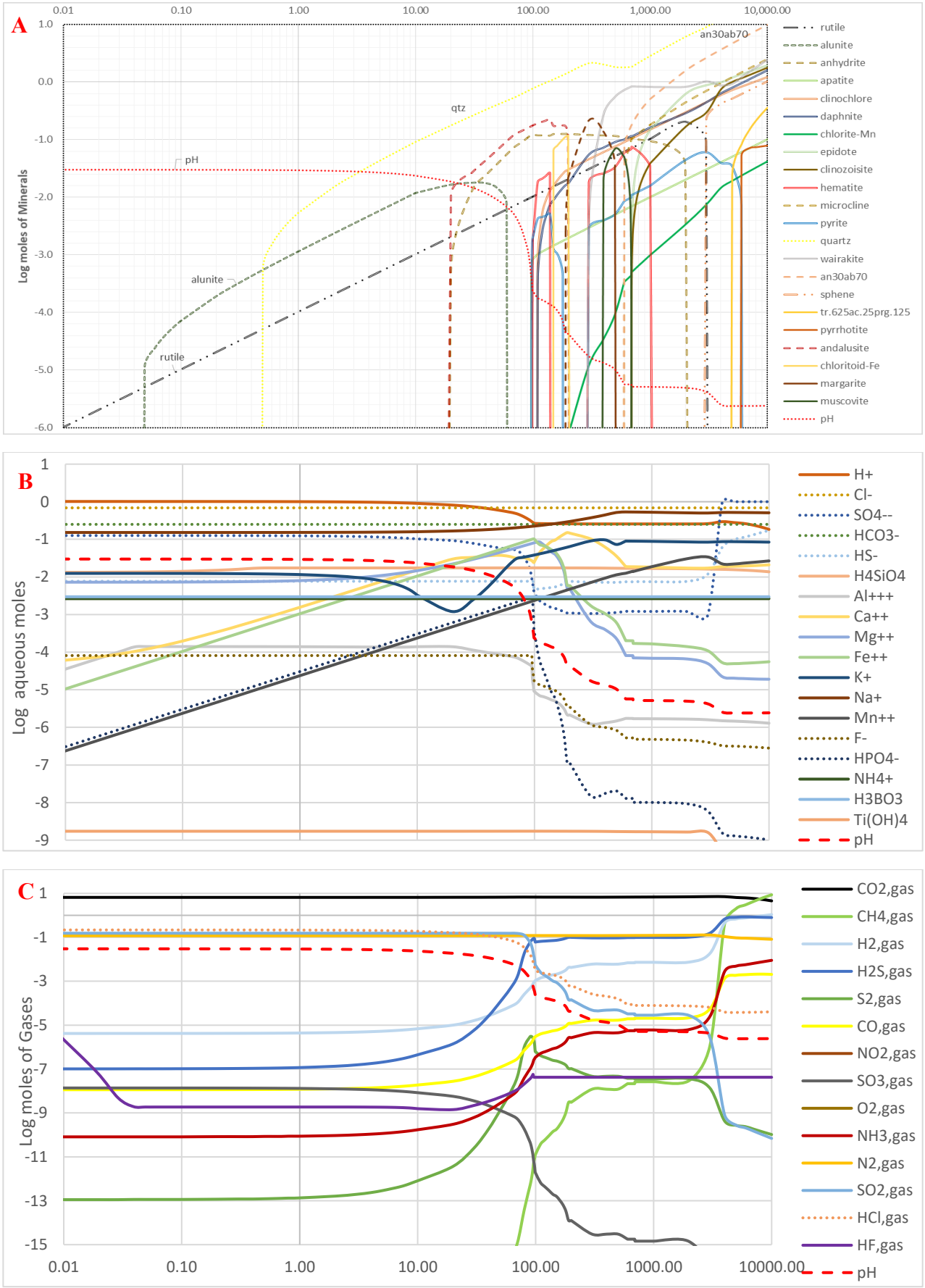

Figure 7: Reaction of the acidic primary fluids at 500°C with the andesitic wall rock. Abscissa shows the amount of andesite (in grams) titrated into one kilogram of the fluid.
A. Alteration minerals
B. Total molality of major component species (H_2O off scale at the top)
C. Gas phase composition (O2 and NO2 gas off scale at the bottom)

$$Fe_2O_3 + 2Al^{3+} + H_4SiO_4 + 0.25HS^- \rightarrow FeAl_2SiO_7H_2 + 0.25SO_4^{2-} + 4.25H^+$$
$$(hem, s)\ (aq)\quad (Qtz, s)\quad (aq)\quad (chloritoid\text{-}Fe, s)\quad (aq)\quad (aq) \qquad (5)$$

This is then followed by a sudden decrease in pyrite concentration along with andalusite being replaced by margarite where a bigger change in pH (4 immediately jumping to 4.3) occurs (equation 6; Figure 7A). The pH is mainly controlled by the activity of Ca^{2+} and Al^{3+}. The occurrence of these two minerals act as a pH buffer (at pH 4.4) which is short-lived (note that the scale may not be too obvious in the graphs) since it immediately fails after andalusite production stops, thus the reaction proceeds to the right.

$$Al_2SiO_5 + 2Al^{3+} + H_4SiO_4 + 3H_2O + Ca^{2+} = CaAl_4Si_2O_{12}H_2 + 8H^+$$
$$(andalusite, s)\ (aq)\quad (qtz, s)\quad (aq)\quad (aq)\quad (margarite, s)\quad (aq) \qquad (6)$$

Simultaneous formation of hematite, pyrite and large amounts of wairakite is observed at 300 grams of andesite reacted. Reversal of Hematite-Cloritoid-Fe reaction (equation 5) is observed since hematite is reproduced again in the system. pH is continuously increasing as these minerals form. At this point, margarite is also seen to have its peak amount followed by a sudden decrease in abundance which is opposite to wairakite's trend. A few more increments of rock added in the system (400 grams), muscovite starts to form. At this point, margarite formation halts while feldspars such as plagioclase member ($an_{30}ab_{70}$) and microcline starts to form. pH remains at 5.25 (Appendix B) while muscovite and the feldspars are produced making them mineral buffers as shown in equation 7 and 8.

$$KAl_3Si_3O_{12}H_2 + 4.8H^+ + 0.7Na^{2+} + 0.3Ca^{2+} = Na_{0.7}Ca_{0.3}Al_{1.3}Si_{2.7}O_8 + 2.8H_2O + K^+ + 1.7Al^{3+} + 0.3H_4SiO_4$$
$$(muscovite, s)\quad (aq)\quad (aq)\quad (aq)\quad (an30ab70, s)\quad (aq)\quad (aq)\quad (aq)\quad (qtz, s) \qquad (7)$$
$$KAl_3Si_3O_{12}H_2 + 6H^+ = KAlSi_3O_8 + 4H_2O + 2Al^{3+}$$
$$(muscovite, s)\quad (aq)\quad (microcline, s)\quad (aq)\quad (aq) \qquad (8)$$

As muscovite production stops, a small increase in pH is observed (from 5.25 to 5.28 as seen in Appendix B) along with the formation of epidote and clinozoisite at around 700 grams rock. The relationship is shown in equations 9 and 10.

$$KAl_3Si_3O_{12}H_2 + Fe^+ + 0.125SO_4^{2-} + 2Ca^{2+} \rightarrow Ca_2Al_2FeSi_3O_{13}H + 0.125HS^- + K^+ + Al^{3+} + 1.875H^+$$
$$(muscovite, s)\quad (aq)\quad (aq)\quad (aq)\quad (epidote, s)\quad (aq)\quad (aq)\quad (aq)\quad (aq) \qquad (9)$$
$$KAl_3Si_3O_{12}H_2 + H_2O + 2Ca^{2+} \rightarrow Ca_2Al_3Si_3O_{13}H + K^+ + 3H^+$$
$$(muscovite, s)\quad (aq)\quad (aq)\quad (clinozoisite, s)\quad (aq)\quad (aq) \qquad (10)$$

At 1000 grams, hematite productions halts. Similarly, anhydrite also stops at around 2000 grams. However, pH remains constants as the w/r progresses despite the disappearance of these minerals. Quartz, feldspars, chlorites and other silicates are still continuously produced. At a very large water-rock interaction (around 3000 grams), rutile formation stops and is replaced by sphene. This interaction is shown in equation 11. In figure 7A and Appendix B, this w/r ratio marks a slight increase in pH (5.3 to 5.6) thus an indication that the buffers which kept the pH stable from 700 to 3000 grams of rock interacted eventually fails along with the disappearance of rutile. As shown, in equation 11, the pH is highly related to the activity of Ca^{2+}. Along with the rutile-sphene replacement, clinozoisite is also observed to greatly increase at this w/r ratio.

$$TiO_2 + H_4SiO_4 + Ca^{2+} \rightarrow CaTiSiO_5 + H_2O + 2H^+$$
$$(rutile, s)\ (qtz, s)\quad (aq)\quad (sphene, s)\ (aq)\quad (aq) \qquad (11)$$

$Tr_{.625}ac_{.25}par_{.125}$ forms at 5000 grams. The last mineral to form at very high water rock interaction is pyrrothite (at around 6000 grams) which replaces pyrite. In this condition, the pH change is very minute.

$$FeS_2 + H_2O = FeS + 0.75HS^- + 1.25H^+ + 0.25SO_4^{2-}$$
$$(pyrite, s)\ (aq)\ (pyrr, s)\quad (aq)\quad (aq)\quad (aq) \qquad (12)$$

At the maximum w/r ratio (10000 grams of andesite reacted with acidic water) the assemblage constitutes, quartz, plagioclase ($an_{30}ab_{70}$), wairakite, epidote, clinozoisite, chlorite end members (clinochlore, daphnite and chlorite-Mn), sphene, $tr_{.625}ac_{.25}par_{.125}$, apatite, pyrrothite and fluoroapatite. The ending pH is at 5.6 from the initial pH of 1.5 at the start of the titration process.

5. SUMMARY

Interaction between acidic water and andesite would form several silicate minerals along with some oxides, hydroxides, sulphates and sulfides. These minerals are related to the change in pH as such minerals would consume or liberate certain ion species that will affect the activity of H^+. As the water-rock ratio progresses, more minerals are produced. In the case of acidic fluid and andesite reaction, more drastic changes occurs as more minerals form. Initially, rutile forms followed by alunite and quartz at smaller w/r ratio where very small changes in pH happens up until the formation of anhydrite and andalusite. The most drastic changes in the pH happens between 100 to 1000 mg rock added. This is attributed to the formation of certain minerals and failure of several short-lived mineral and ion buffers.

REFERENCES

Apuada N.A. and Sigurjonsson G.F.: The Geothermal Potential of Biliran Island, Philippines. *Proceedings*, 8th Asian Geothermal Symposium, Vietnam Institute of Geosciences and Mineral Resources (VIGMR), Hanoi city, Vietnam (2008)

Balangue-Tarriela M.D.: Chemical Reaction Path Modeling of Hydrothermal Mineralization in the Tongonan Geothermal Field, Leyte (Philippines). *Geothermics*, **33**(1-2), (2004), 143 – 146.

Bartolo, E.A. and Reed, M.H.: Geochemical Modeling of Acidic Geothermal Fluids using SOLVEQ and CHIM-xpt. *Proceedings*, World Geothermal Congress, Melbourne, Australia (2015).

Bjornsson A. and Sarmiento, Z.: Biliran I and II Updated Resource Assessment after Drilling Well BN-8. Report No 100054-03. *Unpublished company report* (2015).

Cabahug, M.S. and Angcoy Jr., E.C.: Modeling the reservoir fluids of acidic geothermal wells in Mahanagdong, Leyte, Philippines. *Proceedings,* Fourteenth International Symposium on Water-Rock Interaction, Palais des Papes, Avignon, France (2013).

FILTECH Energy Drilling Corp. (FEDCO): Resource Assessment: The Biliran Geothermal Field, Philippines. *Unpublished company report* (2009).

Giggenbach W.F.: Geothermal mineral equilibria, *Geochimica et Cosmochimica Acta*. **45**(3), (1981), 393–410.

Harvey C.C.: Water-Rock Interaction, Alteration Minerals and Mineral Geothermometry. IGA Academy Report 0111-2013 (2013).

Licup, A.C. and Omac X.L.: Geology of BN-6. Biliran Geothermal Incorporated. *Unpublished company report*. (2014).

Pagado E.S., Camit, G.R.A., Rosell, J.B. and Apuada, N.A.: The Geology and Geothermal Systems of Biliran Island*, Journal of the Geological Society of the Philippines*, **5**(1), (1995), 21-36.

Pang, Z. and Reed, M.: Theoretical Chemical Thermometry on Geothermal Waters: Problems and Methods. *Geochimica et Cosmochimica Acta*, **62**(6), (1998), 1083-1091.

Ramos-Candelaria M.N., Ruaya J.R. and Baltasar A.S.J.: Geochemical and Isotopic Investigation of Biliran Geothermal Discharges, Philippines. IAEA-TECDOC-788 (1993).

Reyes, A.G. 2015. A Petrological Evaluation of Well BN-6D, *GNS Science Consultancy Report 2015/105*, 10 p, (2015).

Reed M.H. and Spycher N.F.: Calculation of pH and mineral equilibria in hydrothermal water with application to geothermometry and studies of boiling and dilution. *Geochima Cosmochima Acta*, **48**, (1984), 1479-1490.

Reed, M.H., Spycher, N.F. and Akaku, K.: Numerical Models of Boiling and Mixing in Geothermal Waters. *Proceedings*, International Geothermal Association. 51-58, (1988).

Reed M.H.: Computer Modelling of Chemical Processes in Geothermal Systems: Examples of Boiling, Mixing and Water-Rock Reaction. *Proceedings*, Application of Geochemistry in Geothermal Reservoir Development, United Nations Institute for Training and Research, United Nations Development Program, N.Y., 275-298, (1992).

Reed M.H.: Hydrothermal alteration in active continental hydrothermal systems, in Short Course Notes – Geological Association of Canada; 11; 315-338; Alteration and alteration processes associated with ore-forming systems, (1994).

Reed, M.H., Spycher, N.F. and Palandri J.: Users Guide for CHIM-XPT: A Program for Computing Reaction Processes in Aqueous-Mineral-Gas Systems and MINTAB Guide (Version 2.43). Department of Geological Sciences, University of Oregon, Eugene, Oregon, USA, (2012).

Reyes A. G.: Petrology of Well Biliran-1. *Unpublished PNOC EDC Report*, (1982).

Reyes A.G.: Petrology of Philippine Geothermal Systems and the application of Alteration Mineralogy to their Assessment. *Journal of Volcanology and Geothermal Research,* **43**, (1990), 279-309.

Reyes, M.V. and Ordoñez, E.P.: Philippine Cretaceous smaller foraminifera. *Journal of the Geological Society of the Phil*ippines, **24**(2), (1970), 1-13.

Zhang Z,: Water-Rock Interaction in the Bakki Low Temperature Geothermal Field SW-Iceland. *Proceedings*, United Nations University Geothermal Training Programme 2001 – Report 17, Reykjavik, Iceland, 405-432 (2001).

APPENDIX A

Sample Run file (CHIMRUN.DAT) for modeling the acidic water- andesitic rock interaction.

```
Biliran Andesite + Acidic Water, w/ 27 g 75/25Wt%, frac 0.00095 g qz.


<  erpc  ><    pH    >< pfluid ><  temp  ><  tempc ><  volbox-1  ><rhofresh>< rhorock>
 0.100E-11    0.0000  500.0000  350.0000    0.0000   1.000000      0.000      2.500

< step increm >< step limit  >< total mixer >
 0.0010000        0.0100       0.0000000

<  enth   ><  senth  ><  denth  ><  totwat >< solmin ><   rm    ><  aqgrm >< suprnt >
     0.0000     0.0000     0.0000    90.0000 0.000E+00    0.0000    0.0000 0.100E-21

l/v:0  chg    i    i    n    i  lim         i   it    i    i   in incr  min         a
hiP:1  bal frac punc loop step  sol looc enth  ref deal psat crem    P solv neut watr
    0    3    0    1  400    2    1    0    0    0    0    1    0    0    1    0    0

 saq> <   name    ><   total moles   >< trial molality  ><       gamma     ><mixer total
    1 H+            1.01517755470     0.269841399968     0.393251918839      0.00000000
    2 H2O           1.37963422915      1.00000000000     0.981654937996      0.00000000
    3 Cl-          0.687272693363     0.292105281830     0.369076565070      0.00000000
    4 SO4--        0.126002430669     0.763669156910E-05 0.237229038460E-01  0.00000000
    5 HCO3-        0.249800000000     0.129003731135E-07 0.389562417087      0.00000000
    6 HS-          0.766500000000E-02 0.113110633424E-10 0.371301402364      0.00000000
    7 H4SiO4       0.131300000000E-01 0.948133571999E-02  1.00000000000      0.00000000
    8 Al+++        0.100000000000E-20 0.134547465032E-22 0.171819046233E-03  0.00000000
    9 Ca++         0.456600000000E-04 0.844037966621E-05 0.202324594125E-01  0.00000000
   10 Mg++         0.723900000000E-02 0.275654045212E-02 0.175593920225E-01  0.00000000
   11 Fe++         0.100000000000E-12 0.798006558107E-21 0.182023181692E-01  0.00000000
   12 K+           0.124300000000E-01 0.810158374465E-02 0.396436890093      0.00000000
   13 Na+          0.152000000000     0.776608325691E-01 0.372059347801      0.00000000
   14 Mn++         0.100000000000E-20 0.123225382647E-23 0.186865832303E-01  0.00000000
   23 F-           0.810600000000E-04 0.122918708655E-08 0.328851039306      0.00000000
   27 HPO4--       0.100000000000E-12 0.172470518803E-31 0.238089243703E-01  0.00000000
   32 NH4+         0.264300000000E-02 0.419077958562E-05 0.398978429513      0.00000000
   33 H3BO3        0.296900000000E-02 0.214395169484E-02  1.00000000000      0.00000000
   34 Ti(OH)4      0.100000000000E-12 0.722112402597E-22  1.00000000000      0.00000000

<     minerals     >  < min trial moles>

<    reactants     >  < weight percent ><  ppm? >
SiO2                                57.61
TiO2                                0.825
Al2O3                               18.04
FeO                                 7.552
MnO                                 0.168
MgO                                 2.990
CaO                                 8.500
Na2O                                2.270
K2O                                 1.220
H2O                                 0.430
P2O5                                0.216

< mins to suppress >
kf-ab-equil
FMQ_HS-1
antigorite
riebeckite
an20ab80
an25ab75
bastnaesite-Ce
parisite-Ce

< don't fractionate>

<  T-P curve data  >
```

APPENDIX B

Alteration mineral assemblage at 100 to 10000 grams of andesite reacted to acidic water